Hybrid kinetic-MHD modeling of alpha-driven TAEs in the SPARC tokamak

R.A. Tinguely[1]†, J. Gonzalez-Martin[2]†, and Y. Todo[3]

[1] Plasma Science and Fusion Center, Massachusetts Institute of Technology, Cambridge, MA, USA

[2] Universidad de Sevilla, Seville, Spain

[3] National Institute for Fusion Science, Toki, Gifu 509-5292, Japan

Abstract. As the magnetic confinement fusion community prepares for the next generation of fusion devices and burning plasmas, there is still a question of whether fast ions (FIs) will drive MHD instabilities, causing significant redistribution or even loss of FIs, thereby leading to reduced plasma performance and possibly threatening the integrity of the first wall. In this paper, we explore the existence and stability of Toroidicity-induced Alfvén Eigenmodes (TAEs) in the >100 MW, $Q \sim 9-11$ DT-fusion power "Primary Reference Discharge" (PRD) of the SPARC tokamak; the PRD has a relatively low on-axis alpha pressure, $\beta_{\alpha 0} \approx 0.6\%$, due to the high magnetic field strength, $B_0 = 12.2$ T. A scan in toroidal mode number is performed in the vicinity of the estimated "most unstable" modes, $n \approx 5 - 20$, with the linear eigenvalue code NOVA-K and nonlinear initial-value code MEGA. Both codes identify the same (even) $n = 10$ TAE located near $q = 1$ with frequency $f \approx 360$ kHz and alpha drive $\gamma/\omega \approx +0.6\%$. While MEGA evaluates this mode to be marginally unstable for the nominal alpha pressure, NOVA-K instead identifies a higher frequency (odd) $n = 10$ TAE as marginally destabilized; different evaluations of radiative damping are likely the cause of this discrepancy. These results indicate that AEs may be only marginally unstable for the highest performing SPARC PRD, at least for the q profile explored here. They also serve as a starting point for further scans, inclusion of FIs from auxiliary heating systems, and exploration of AE-induced FI transport, as well as a guide for diagnostic measurements of these $n \approx 10$ AEs.

Keywords: Alfvén eigenmodes, stability, SPARC, NOVA-K, MEGA

1. Introduction

It has been observed in many tokamaks that fast ions (FIs), with velocities of order the Alfvén speed, can destabilize Alfvén eigenmodes (AEs) and that, in turn, these AEs can be correlated with FI transport and deconfinement; for examples, see [1–3] and others. Such FI redistribution in phase space, caused by wave-particle resonances and energy exchange, could thus affect - and possibly degrade - plasma heating, which is usually the goal of the FIs

†Shared first authorship.

in the first place. Of particular interest is the 3.5 MeV alpha particle born in the deuterium-tritium (DT) fusion reaction, which slows down from its birth velocity $v_0 \approx 1.3 \times 10^7$ m/s via collisions. Both TFTR and JET, the only two tokamaks to have operated with DT fuel, have some evidence of alpha-driven AEs [4–6]. However, in those experiments, the alpha populations - and power - were relatively small, with plasma fusion gains $Q < 1$.

An area of active study, therefore, is the prediction of AE stability, alpha drive and transport in the burning plasmas ($Q > 5$) of future DT devices. Many analyses have been carried out for ITER (see [7, 8] and others); this paper focuses on the SPARC tokamak [9], which is currently under construction by Commonwealth Fusion Systems. SPARC is a compact device with major and minor radii $R_0 = 1.85$ m and $a = 0.57$ m, respectively; its high magnetic field strength $B_0 = 12.2$ T and plasma current $I_\mathrm{P} = 8.7$ MA are enabled by high temperature superconducting technology [10]. These strong fields, together with relatively large plasma densities $O(10^{20}$ m$^{-3})$, yield a high Alfvén velocity $v_\mathrm{A} \approx 9 \times 10^6$ m/s, which yet is still less than the alpha birth velocity.

Previous works have considered AE stability and related transport in SPARC: In [11], the authors investigated trends of parameters relevant to AE stability with the magnetic field strength B: e.g. alpha pressure; AE mode structures, growth rates, resonance conditions; and more. A scan in B was performed using a suite of codes: HELENA [12] to compute the magnetic equilibrium, MISHKA [13] to identify AEs, and CASTOR-K [14] to evaluate AE growth (and damping) rates. Importantly, a notional set of profiles (scaled from an Alcator C-Mod discharge) was used, simply because the paper was published before the SPARC Physics Basis [9]. In addition, only alpha drive and ion Landau damping were included in the stability calculation, without any finite Larmor radius (FLR) effects.

A drift kinetic theory of alpha transport was derived in [15] and applied to cases of toroidal magnetic field ripple and a generic Toroidicity-induced AE (TAE) in SPARC. Reference [16] complemented this work with a numerical investigation of ripple-induced alpha transport, comparing the ASCOT5 [17] and SPIRAL [18] orbit-following codes. Further numerical analysis of TAE-induced alpha transport is underway, but will be left for a future publication.

This work presents the most thorough analysis to date of alpha-driven TAEs in SPARC. We improve upon [11] by analyzing a realistic magnetic geometry and set of plasma profiles for SPARC [19], given in Section 2. Furthermore, Section 3 complements the stability analysis of [11] using the linear eigenvalue solver and stability code NOVA-K [20–22] which includes additional drive and damping mechanisms as well as FLR effects. We then compare linear results to those from the nonlinear code MEGA [23] in Section 4. Finally, Sections 5 and 6 provide a discussion and summary.

2. Modeling inputs

The magnetic geometry, plasma profiles, and FI distribution functions are common inputs to both codes. Specifically, the scenario of interest is SPARC's planned highest performing

"Primary Reference Discharge" (PRD), a double-null H-mode DT plasma with maximum fusion power $P_{\text{fus}} = 140$ MW [9, 19, 24]. Of course, a plasma with maximal DT fusion power also has the highest alpha particle generation rate, which is why the PRD is the most relevant scenario for initial exploration of alpha-driven AEs in SPARC. Other plasma scenarios could lead to even greater alpha drive or a wider variety of FI-related instabilities, as discussed later; however, we decide to focus on the PRD, the SPARC scenario most explored to date.

The first high fidelity simulations of core plasma performance for the PRD were carried out in [19]; figure 7 within shows the time-evolution of the standard baseline discharge, including the sawtooth instability. During the quasi-quiescent period between sawtooth crashes, there is minimal change in the on-axis and volume-averaged electron densities, while the on-axis electron and ion temperatures vary by roughly ∼10%. Of course, the sawtooth crash affects the temperatures greatly, reducing them by almost a factor of 2, along with the requisite change in the core safety factor (q) profile, i.e. the existence and movement of the $q = 1$ surface. It is primarily computational resources that limit the following simulations of Sections 3 and 4 to a single time slice, and we simply choose a time shortly before a sawtooth crash, which is explored further in [19] and in many follow-on publications. It is difficult to quantify uncertainties introduced by selecting this single time; however, we posit a rough ∼10% uncertainty in relevant plasma parameters (neglecting the effect of sawteeth) and discuss the resulting uncertainty propagation in later results.

Electron and ion density and temperature profiles from TRANSP [25–27] simulations are shown in Fig. 1 for the single time selected, along with the q profile before the sawtooth crash. In the figures, ψ_{N} is the normalized poloidal flux, and $\sqrt{\psi_{\text{N}}}$ is approximately the normalized minor radius (i.e. $\sqrt{\psi_{\text{N}}} = \rho_{\text{pol}} \sim r/a$). A poloidal cross-section of $\sqrt{\psi_{\text{N}}}$ is depicted in Fig. 2, along with the reduced-resolution, field-aligned grid used in MEGA. Uniform $Z_{\text{eff}} = 1.5$ and $(n_D + n_T)/n_e = 0.85$ were assumed in the TRANSP simulations, with an impurity mix that consists of the Helium-3 (He3) minority, tungsten (W), and a lumped low-Z impurity (F). An effective density, incorporating dilution as well as the two main ion species of different masses, is used in the following simulations of Sections 3 and 4. We note, however, that the correction to the Alfvén speed and frequencies due to this dilution is <5%.

Here, it is important to discuss the q profile used for modeling. From the analysis of [19, 24], the sawtooth period is ∼1 s, similar to the energy confinement time of ∼0.8 s and ∼4× the alpha slowing down time, meaning that the plasma is approximately in steady state before the sawtooth crash. At the selected time slice, the rational surface $q = 1$ is located at mid-radius, around $\sqrt{\psi_{\text{N}}} \approx 0.5$, as seen in Fig. 1a. Because this time is just before the sawtooth crash, the $q = 1$ surface is likely near the largest radius at which it will exist, at least during the flat-top plasma current of the SPARC PRD scenario. For this reason, the chosen time slice has an "extreme" $q = 1$ location, which affects the existence of AEs and their stability. We discuss the impact of this choice in the following sections, and other q profiles should be investigated in future work.

The SPARC PRD will be externally heated by ∼11 MW of ion cyclotron radio frequency (RF) power, utilizing He3 as the minority ion species [28]. In the TRANSP simulation used

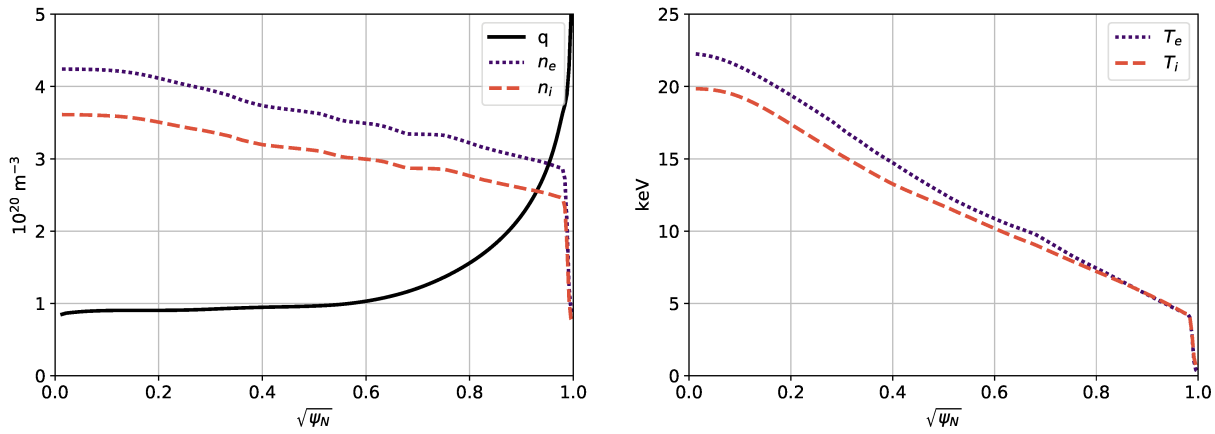

(a) (b)

Figure 1: (a) Density and (b) temperature profiles, from TRANSP, for electrons (dotted) and ions (dashed) in the SPARC Primary Reference Discharge (PRD), plotted vs normalized minor radius $\sqrt{\psi_{\rm N}}$, with $\psi_{\rm N}$ the normalized poloidal flux. Note that $n_i = n_D + n_T$ is the combined D+T ion density. The safety factor profile (solid) is also shown in (a).

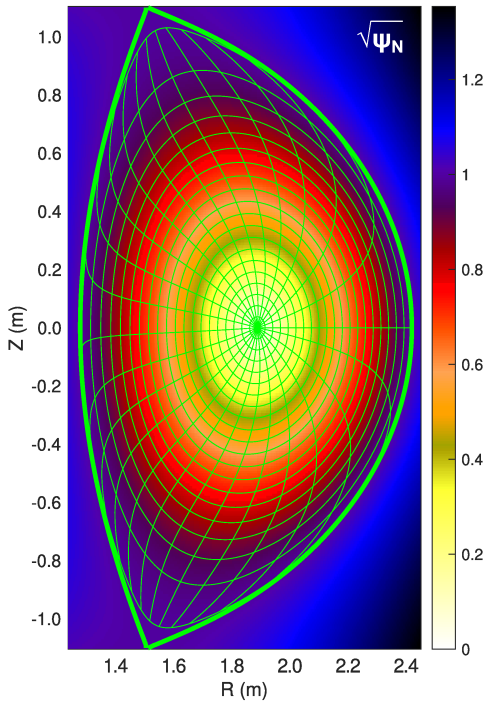

Figure 2: A poloidal cross-section of the SPARC PRD magnetic equilibrium, showing the square root of normalized poloidal flux $\sqrt{\psi_{\rm N}}$ together with the field-aligned grid used for post-processing in MEGA, with a reduced resolution for visualization.

here, the total fusion power is ∼111 MW and Ohmic heating is ∼1 MW, meaning that alpha power will contribute ∼22 MW of self-heating to this $Q \approx 9$ plasma. The normalized pressure (β) profiles for the main and FI species are shown in Fig. 3a. All values are relatively low due to the high magnetic pressure. The central β_0 is actually larger for the He3 RF minority than alphas, i.e. ∼1% compared to ∼0.6%. However, the alpha profile is much broader, with a fairly constant radial gradient to mid-radius ($\sqrt{\psi_N} \approx 0.1 - 0.5$), whereas the He3 FI gradient is steepest within the core ($\sqrt{\psi_N} < 0.2$), as shown in Fig. 3b. Note that the small positive gradient for the alphas at the plasma center ($\sqrt{\psi_N} < 0.1$) is not real, but due to poor marker statistics in the NUBEAM simulation [29].

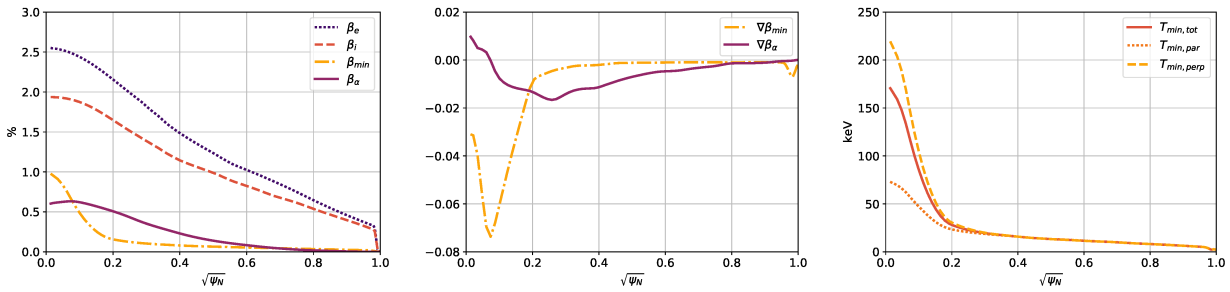

(a) (b) (c)

Figure 3: (a) Normalized pressure (beta) profiles, from TRANSP, for electrons (dotted), ions (dashed), Helium-3 RF minority ions (dot-dashed), and alphas (solid) in the SPARC PRD. (b) Gradients of He3 and alpha betas from (a). (c) Total (solid), parallel (dotted), and perpendicular (dashed) effective temperatures for the He3 RF minority population vs normalized minor radius $\sqrt{\psi_N}$.

The alpha population, computed by NUBEAM, is isotropic in pitch angle and exhibits the usual slowing down distribution in velocity. The He3 population from TORIC-FPP [30, 31], on the other hand, is quite anisotropic. The total, parallel, and perpendicular "effective" temperature profiles are plotted in Fig. 3c. Note the similarity to Figure 13 in [16]. These data are used in Section 3 to evaluate the RF contribution to linear AE stability with NOVA-K where, at each radial location, the RF tail is modeled with an anisotropic equivalent temperature [32]. As will be seen, these RF-accelerated FIs are not expected to destabilize mid-radius TAEs, so the follow-on nonlinear MEGA calculations in Section 4 only simulate the alphas. The study of RF drive, perhaps of energetic particle modes, will be pursued in future work, and is further discussed in Section 5.

In both NOVA-K and the single-n version of MEGA - as well as most, if not all, other AE stability codes, the toroidal mode number n is also an input value. Therefore, we are interested in modeling the "most unstable" n. As in other works [7, 11, 15, 16, 33], this is computed from the resonance condition, equating the mode and particle orbit widths. The

mode width is approximated as

$$\Delta_{\rm m} \approx \frac{r_{\rm m}}{m} \approx \frac{r_{\rm m}}{nq(r_{\rm m})}, \tag{1}$$

where m is the poloidal mode number and $q(r_{\rm m})$ is the safety factor at the mode minor radial location $r_{\rm m}$. The orbit width is

$$\Delta_{\rm o} \approx \frac{qv_{\parallel}}{\omega_{\rm FI}} = \frac{qm_{\rm FI}v_{\parallel}}{Z_{\rm FI}eB}. \tag{2}$$

Here, the FI is characterized by its parallel velocity $v_{\parallel}$, gyrofrequency $\omega_{\rm FI}$, electric charge $Z_{\rm FI}e$, and mass $m_{\rm FI}$. From Eqs. (1) and (2), the most resonant toroidal mode number is given by

$$n^* \approx \frac{Z_{\rm FI}e}{m_{\rm FI}}\frac{Br_{\rm m}}{q^2v_{\parallel}}. \tag{3}$$

There are a few free choices here: First is the mode location, which we can estimate to be at mid radius, $r_{\rm m} \approx a/2$. For TAEs, the primary resonance is at the Alfvén speed, $v_{\parallel} = v_{\rm A}$. Plugging in values for alpha-driven TAEs in SPARC gives $n^* \approx 8-18$ for $q = 1-3/2$. While this is a relatively wide range, it at least provides a starting point for simulation scans.

3. Linear modeling with NOVA-K

3.1. TAE existence and stability

The eigenvalue solver NOVA-K [20–22] is first used to compute all possible AE mode structures and eigenfrequencies among the Alfvén continua. Profiles from Section 2 are provided as inputs. A fit to the magnetic equilibrium is performed internally in NOVA-K, with the magnetic axis, last closed flux surface, and q profile serving as constraints (see Figs. 1a and 2). No toroidal rotation is considered here, but its expected effect would only be to add a Doppler shift to the frequency. A coarse scan in toroidal mode number is performed: $n = 5, 10, 15$ and 20. This is chosen to cover the range of most unstable mode number n^* predicted in Section 2; however, the upper bound is ultimately limited by the need for finer radial resolution with increasing n and resulting computational expense.

Of all AE solutions, a subset is chosen based on (i) eigenfrequencies within the TAE gap and (ii) mode structures minimally intersecting with the Alfvén continuum. Representative low and high frequency AEs - i.e. even and odd modes - are selected for stability analysis, near the bottom and top of the TAE gap, respectively; their poloidal mode structures are shown in Fig. 4. Note that the modes are localized near the flux surface $q = 1$, i.e. with dominant poloidal harmonics $m, m+1 \approx n$. Only the $n = 5$ TAEs, with broadest mode widths, seem to have significant interactions with the Alfvén continuum. Other TAEs at higher $q > 1$, i.e. $\sqrt{\psi_{\rm N}} > 0.5$ (see Fig. 1a), would intersect the continuum and likely have too high damping; thus, they are not assessed here.

NOVA-K is then used to calculate the linear stability of each AE from a variety of drive and damping mechanisms. Table 1 gives a breakdown of all contributions, with growth rates $\gamma > 0$ normalized to each eigenfrequency $\omega = 2\pi f$. (Note that $\gamma/\omega < 0$ indicates

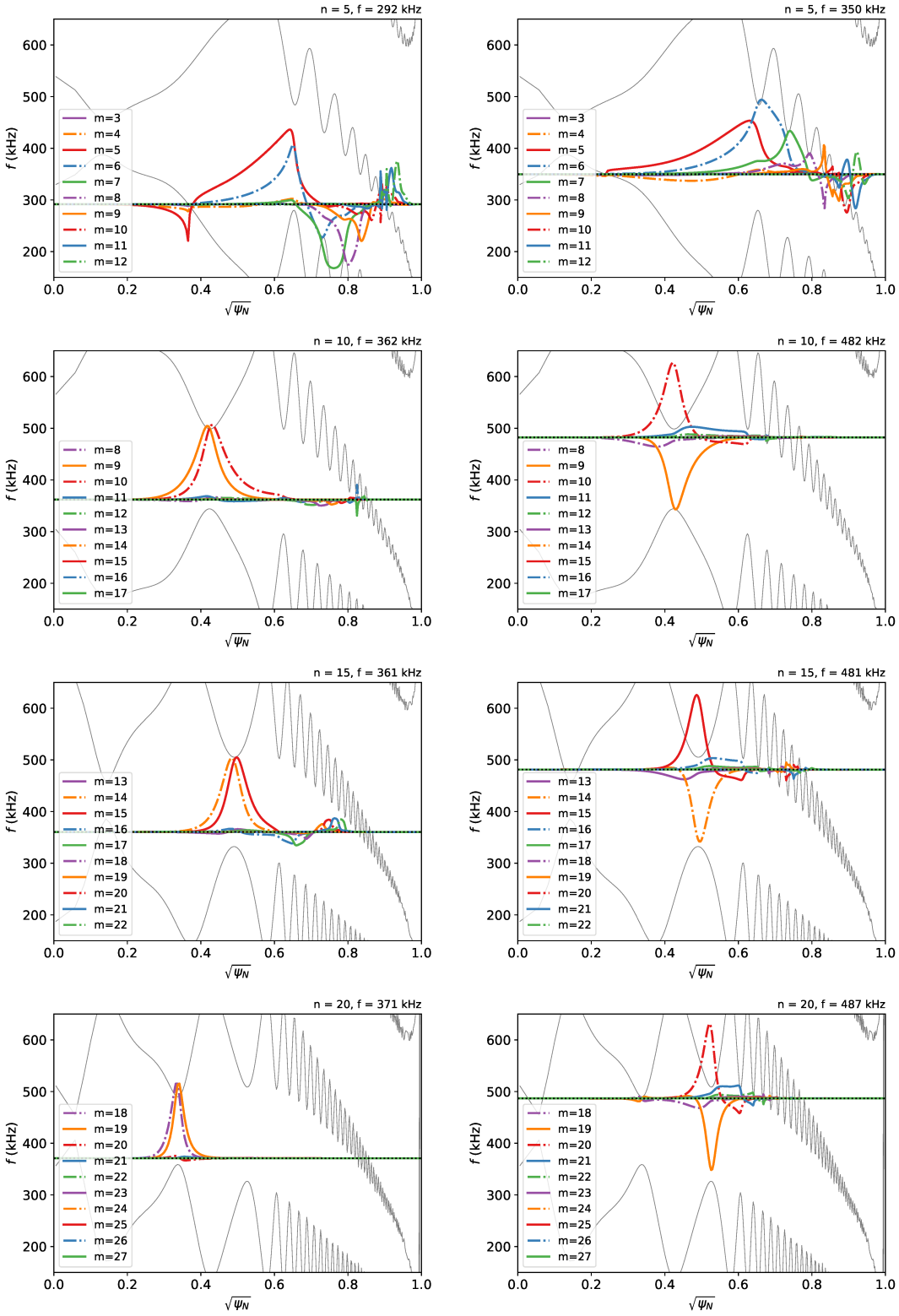

Figure 4: NOVA: Poloidal mode structures (m, solid and dot-dashed) vs normalized radius for AEs with toroidal mode numbers $n = 5, 10, 15$, and 20. For each n, low and high frequency modes (horizontal lines) are shown within TAE gaps of the Alfvén continua (thin lines).

Table 1: NOVA-K: Eigenfrequencies and normalized growth rates γ/ω [%] (damping < 0) for AEs with toroidal mode numbers $n = 5, 10, 15$, and 20. A breakdown of damping and drive mechanisms is provided, with and without finite Larmor radius (FLR) effects. Net growth rates are given with (**bolded**) and without (*italicized*) the contributions from fast ions (FI) *including* FLR effects: RF-accelerated He3 FIs and DT alphas.

n	5		10		15		20	
f (kHz)	292	350	362	482	361	481	371	487
Continuum	−0.06	−0.01	−0.02	−0.00	−0.02	−0.01	−0.00	−0.00
Radiative	−2.69	−0.29	−1.35	−0.00	−0.95	−0.01	−2.63	−0.03
Electron collisional	−0.01	−0.01	−0.02	−0.01	−0.01	−0.01	−0.01	−0.01
Electron Landau	−0.08	−0.13	−0.01	−0.01	−0.01	−0.02	−0.00	−0.01
Ion Landau	−0.02	−0.08	−0.08	−0.03	−0.05	−0.02	−0.08	−0.01
He3 FIs w/o FLR	−0.18	−0.07	−0.20	−0.06	−0.19	−0.08	−0.74	−0.14
He3 FIs w/ FLR	−0.17	−0.07	−0.19	−0.06	−0.17	−0.07	−0.35	−0.11
Alphas w/o FLR	+0.06	+0.01	+0.75	+0.34	+1.01	+0.32	+1.85	+0.22
Alphas w/ FLR	+0.06	+0.01	+0.61	+0.29	+0.79	+0.25	+0.71	+0.13
Total w/o FI	*−2.86*	*−0.44*	*−1.48*	*−0.05*	*−1.04*	*−0.06*	*−2.72*	*−0.06*
Total w/ FI	**−2.98**	**−0.49**	**−1.05**	**+0.18**	**−0.42**	**+0.12**	**−2.35**	**−0.04**

damping.) As expected, the $n = 5$ low-frequency TAE exhibits large continuum damping compared to the $n \geq 10$ modes; however, the high-frequency $n = 5$ mode interestingly does not. Radiative damping [34, 35] dominates for most modes and has a greater impact on the even vs odd modes (i.e. at the bottom vs top of the TAE gaps), as discussed in [36]. Electron and ion Landau damping play a lesser role, with electron collisional damping the smallest. The net damping rate, without the contribution of FIs, is highest for the low-frequency TAEs, $-\gamma/\omega \sim 1\% - 3\%$, while the high-frequency TAEs are only marginally damped, $-\gamma/\omega < 0.5\%$.

NOVA-K models the anisotropic distribution function of RF minority ions using the pressure profile in Fig. 3a and effective tail temperature in Fig. 3c [32]. (FLR effects can also be turned on and off in NOVA-K and will be discussed in the next section.) Interestingly, the He3 minority population is predicted to *damp* all modes. There are several possible explanations for this: First, the He3 FI pressure gradient is steepest in the plasma core, around $\sqrt{\psi_N} \sim 0.1$, whereas the TAEs are located at mid radius. Another reason could be that, given the effective parallel temperature $O(75$ keV), very few He3 FIs will have parallel velocities comparable to the Alfvén speed. This situation could be significantly different for a H-minority species at planned lower-B_0 (8 T) SPARC discharges; that is, H FIs could be ∼70% faster while the Alfvén speed would be ∼30% lower.

Alphas are modeled in NOVA-K again using their pressure profile in Fig. 3a, but now implementing a slowing down distribution in velocity space. Since the alpha birth velocity

exceeds v_A, the alpha population is calculated to *drive* all modes, as expected. In addition, the alpha pressure gradient is low, but fairly constant across the plasma (see Fig. 3b), including the mode locations. An important observation is that the alpha drive is stronger for the $n \geq 10$ TAEs compared to $n = 5$. This agrees with our earlier prediction of the most unstable mode number, from Section 2. The total growth rate, including the contributions of both He3 FIs and alphas with FLR effects, is listed in Table 1. Only the high-frequency $n = 10, 15$ TAEs are assessed to be marginally destabilized, $\gamma/\omega < +0.2\%$, even though the alpha drive is larger for the low-frequency TAEs. Odd TAEs, located at the top of the TAE gap, have been observed before in experiment [37]. However, if the contribution from radiative damping is overestimated by NOVA-K, we might expect low-frequency $n = 10, 15$ TAEs to also be driven unstable.

3.2. Uncertainties and finite Larmor radius effects

Regarding stability, it should be noted that *absolute* uncertainties $\pm 0.1\%$ are expected in NOVA-K's calculation of continuum damping, larger than the values reported in Table 1. In addition, as described in [38], the *relative* uncertainty in radiative damping is of order $\sim$10% when assuming 10% uncertainties in q and T profiles.‡ Electron and ion Landau damping are exponentially sensitive [39] to the ratio of the Alfvén and thermal electron and ion velocities, respectively, making it more difficult to propagate uncertainties here; however, we note that their values in Table 1 are small compared to radiative damping and/or alpha drive for each mode. Finally, electron collisional damping depends on the electron beta and collision frequency (see Eq. 2 in [40]) such that $O(10\%)$ relative uncertainty may also be expected from the already low predicted value. Thus, even including the estimated uncertainties in damping, the overall stability would not change for each mode, with the exception of the high-frequency $n = 20$ TAE, which is already near the marginal stability threshold.

Furthermore, as discussed in Section 2, the sawtooth instability will modify the location of the $q = 1$ surface and AE parameters as a result. At the time of the sawtooth crash, any destabilized TAE near $q = 1$ would likely disappear as $q_0 \sim q_{\min} \sim 1$. Yet as the temperature increases in the core, energetic ion populations re-equilibrate, and the $q = 1$ surface moves outward to mid radius, the TAEs identified by NOVA-K could re-form (which has been observed in experiments before, such as in [41] and others). From Fig. 3, we might actually expect the TAEs to be more strongly driven in the core where the alpha and He3 FI betas and gradients are largest. The time evolution of the q profile and its effect on AE stability will be explored in future work; interestingly, this work may have identified the time when TAEs near $q = 1$ are *least* driven by FIs.

Lastly, we consider FLR effects. The maximum Larmor radii, at the approximate mode location $\sqrt{\psi_N} \sim r/a \sim 0.5$, for 1 MeV He3 FIs and 3.5 MeV alphas are 1.2 cm and 2.6 cm, respectively, which correspond roughly to $\Delta r/a \sim 2.1\%$ and 4.5%. The differences in drive and damping with and without FLR effects are shown in Table 1. Very little effect is seen

‡Note that there is an error in Eq. 1 of [38], which should have each term summed in quadrature.

for He3 FIs' damping of $n = 5 - 15$ TAEs, while the damping *decreases* by $\sim 20\% - 50\%$ for the $n = 20$ TAE when including FLR effects. This is likely due to the mode width decreasing with n (see Fig. 4) and becoming more comparable to the Larmor radius, thereby enhancing FLR effects.

In a similar way, FLR effects grow with n for the alphas, although more significantly than for He3 FIs due to the alpha's larger Larmor radius. For the $n = 20$ TAE, a $\sim 40\% - 60\%$ *decrease* in alpha drive is calculated when adding FLR effects. Thus, we would have *overestimated* the contributions from both He3 FIs and alphas by neglecting FLR effects in our stability calculations; this may have impacted the results of [11] as well. Even so, this would not have changed the conclusions about *total* growth rates for the $n = 5 - 20$ TAEs, except the high frequency $n = 20$ TAE, which would be just marginally unstable, instead of marginally stable.

4. Nonlinear modeling with MEGA

4.1. Numerical methods

The MEGA code [23] is used to self-consistently solve the evolution of kinetic particles and the bulk plasma. The kinetic population modeled by Monte Carlo markers can be electrons [42], thermal ions [43], or fast ions (FIs), as in the simulations discussed in this manuscript. In these runs, the kinetic population is simulated using the δf method, including FLR effects. Realistic injections of particles are available when using the full-f version of the code, which is left for future work, that will simultaneously include both alphas and RF-accelerated FIs.

The bulk plasma is described by the non-linear, full MHD equations, including diamagnetic drift and toroidal flows. MEGA assumes quasineutrality on the MHD grid, providing a single density, velocity, and pressure for both thermal ions and electrons. The coupling between the MHD grid and the kinetic species is included through the energetic particle current density term in the MHD momentum equation. More details on the MHD module of the MEGA code can be found in [44–46].

MEGA has been extensively validated against experimental data. Some examples include reproducing the observation of "abrupt large-amplitude events" in JT60-U [47], the visualization of the AE-induced FI flow using imaging neutral particle analyzers [48–50], the impact of the bump-on-tail of the NBI FI distribution on the TAE growth rate [51], the spectrum of externally applied perturbations on AE stability [52,53], as well as measurements of stable and unstable TAEs using the Alfvén Eigenmode Active Diagnostic in JET [38].

The simulations described here are single-n, in which only a portion of the toroidal geometry of the tokamak ($\phi \in [0, 2\pi/n]$) is simulated, including periodic boundary conditions. While these simulations do not capture the interaction between modes of different toroidicities, they are computationally efficient, as only $N_\phi = 32$ toroidal grid points are required to resolve the instability for $n \leq 16$. The poloidal resolution, $N_R = N_Z = 256$, is set to resolve $n = 10$ perturbations, using the radial profile of the TAEs calculated by NOVA-K

as a mock-up, and comparing against the grid distributions on the poloidal plane (see Figs. 2 and 4).

In these simulations, the frequency of the destabilized modes will depend on the background mass density. As these DT plasmas are expected to have a non-negligible impurity (see Fig. 1a) and $n_{\mathrm{He3}}/n_e = 5\%$ concentration, a correction of 1.15 is applied to the simulated electron density to account for the ratio of the effective density to the bulk deuterium simulated by MEGA.

While the typical on-axis electron temperature for AUG and DIII-D plasmas is about 5 keV [52], the on-axis temperature for this SPARC case is about 20 keV (see Fig. 1b), resulting in a much lower the Spitzer resistivity η_S. Therefore, the simulated value of normalized resistivity is reduced to $\eta_{\mathrm{MEGA}}/(v_A R_0 \mu_0) = 5 \times 10^{-8}$, which is 10× smaller when compared to similar simulations of AUG and DIII-D plasmas [46, 52]. Yet this ensures that the same ratio of the simulated resistivity with respect to the Spitzer resistivity is maintained, about $\eta_{\mathrm{MEGA}}/\eta_S \sim 2000$. This reduction is admissible as the poloidal resolution is increased compared to the AUG and DIII-D simulations, where numerical convergence has been already studied [53]. The values of viscosity and diffusivity are maintained at $\nu = \chi = 5 \times 10^{-7} v_A R_0$, which is the same value reported in [45].

The kinetic population is an isotropic slowing down distribution resulting from alphas generated at 3.5 MeV. The different mass and charge with respect to the bulk plasma is carefully considered when normalizing the inputs. The simulated distribution is isotropic in pitch angle and has the slowed down energy profile depicted in Fig. 5b, which is determined by the space-dependent critical velocity, calculated by MEGA based on the input temperature and density profiles (see Fig. 1). The radial profile of the alpha pressure (β_α) is determined by the quasi-analytic built-in distribution [54],

$$\beta_\alpha(\psi_{\mathrm{N}}) = \beta_{\alpha 0} \exp\left[-\left(\psi_{\mathrm{N}}/\Delta\psi\right)^a\right], \tag{4}$$

where the pressure on axis ($\beta_{\alpha 0} = 0.65\%$), radial gradient scale length ($\Delta\psi = 0.16$), and exponential factor ($a = 1.00$) are adjusted to resemble the TRANSP/NUBEAM outputs, as depicted in Fig. 5a. The on-axis value of normalized alpha pressure ($\beta_{\alpha 0}$) is nearly half of the typical values used for ITER simulations; for instance, $\beta_{\alpha 0} \approx 1.2\%$ was used in [44]. This small value of the normalized pressure, despite the >100 MW of fusion power, is explained by the high magnetic field strength $B_0 = 12.2$ T.

4.2. Marginally unstable $n = 10$ TAE

The single-n simulations described in the previous section are run for longer than $t = 0.22$ ms $= 163\tau_{A0}$, with $\tau_{A0} = 2\pi R_0/v_{A0}$ the Alfvénic period. The increased poloidal resolution requires increased computational resources, so each simulation takes an average of 72 hours using 512 CPUs. The evolution of the $n = 10$ radial velocity perturbation δv_r, once the mode is destabilized, is plotted in Fig. 6a. In this figure, the amplitude at each time step t_k is multiplied by a factor of $\exp(-\gamma t_k)$, with γ an ad-hoc parameter adjusted to visualize

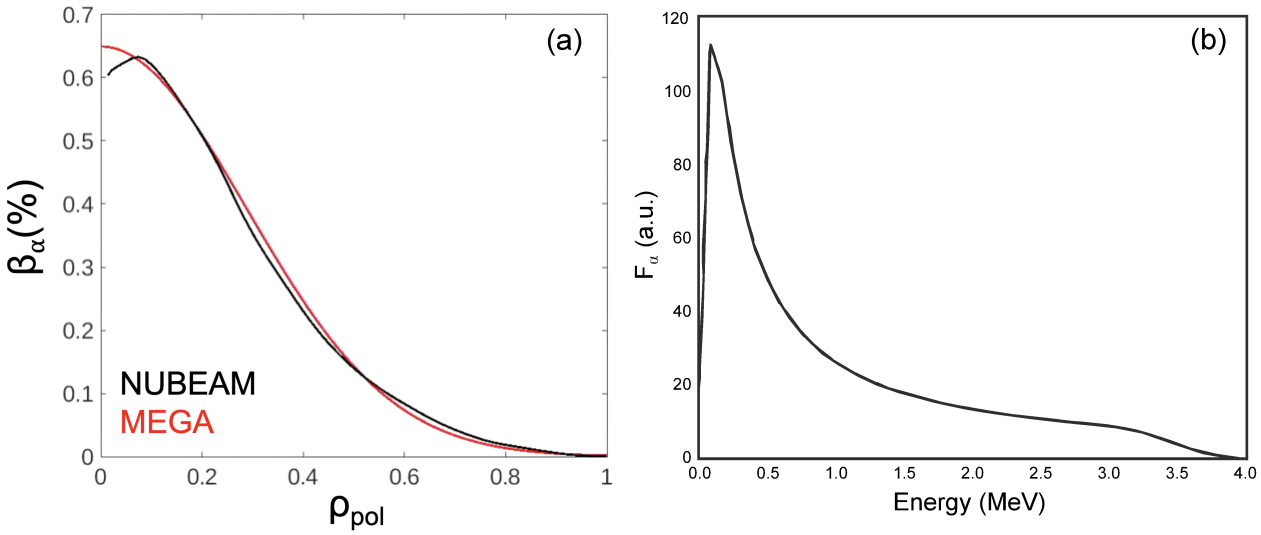

Figure 5: MEGA:(a) Radial profile of the alpha normalized pressure β_α simulated in MEGA, which is adjusted to match the NUBEAM distribution (see Fig. 3a), as a function of normalized radius $\rho_{\rm pol} = \sqrt{\psi_{\rm N}}$. (b) Energy distribution of the alpha particle population.

the evolution of the perturbation; the mode is be observed to oscillate around $\rho_{\rm pol} = 0.38$ for the entire linear phase.

Figure 6b depicts the Fast Fourier Transform (FFT) of the δv_r field, together with the Shear Alfvén Wave (SAW) continuum calculated using the ALCON code [55]. As the linear growing phase is relatively long, the FFT has a good frequency resolution, and we observe the mode located near $f = 370$ kHz, exactly at the location where the $m = 9$ and $m = 10$ even coupling is located [37]. This even coupling of $m = 9, 10$ is even more evident when looking at the poloidal harmonics during the linear phase (Fig. 7), which allows us to classify this mode as a low-shear TAE [56], as only two poloidal harmonics have a significant amplitude. (This region of low shear is also visible in the q profile of Fig. 1a.) Figure 8 depicts the resulting 2D mode structure during the linear phase, including all poloidal harmonics for the fluctuation amplitudes of the radial velocity δv_r, radial magnetic field δB_r, and toroidal electric field δE_ϕ. It is observed that δv_r and δE_ϕ exhibit a ballooning structure while δB_r an anti-ballooning structure, which is expected for an even-parity TAE.

Here, we note that the TAE gap, computed by the 1D ALCON code and shown in Fig. 6b, is just slightly higher in frequency than the FFT analysis of the mode from MEGA. The TAE appears to marginally intersect the continuum at the location with even coupling of $m = 9$ and $m = 10$. However, this small frequency overlap is likely due to different treatments of plasma equilibrium and geometry between the two codes and should not be of any concern here.

Although the simulated TAE has a clear radial structure and frequency, grows at a constant rate, and exhibits a clear $m, m + 1$ coupling, its growth rate is so small

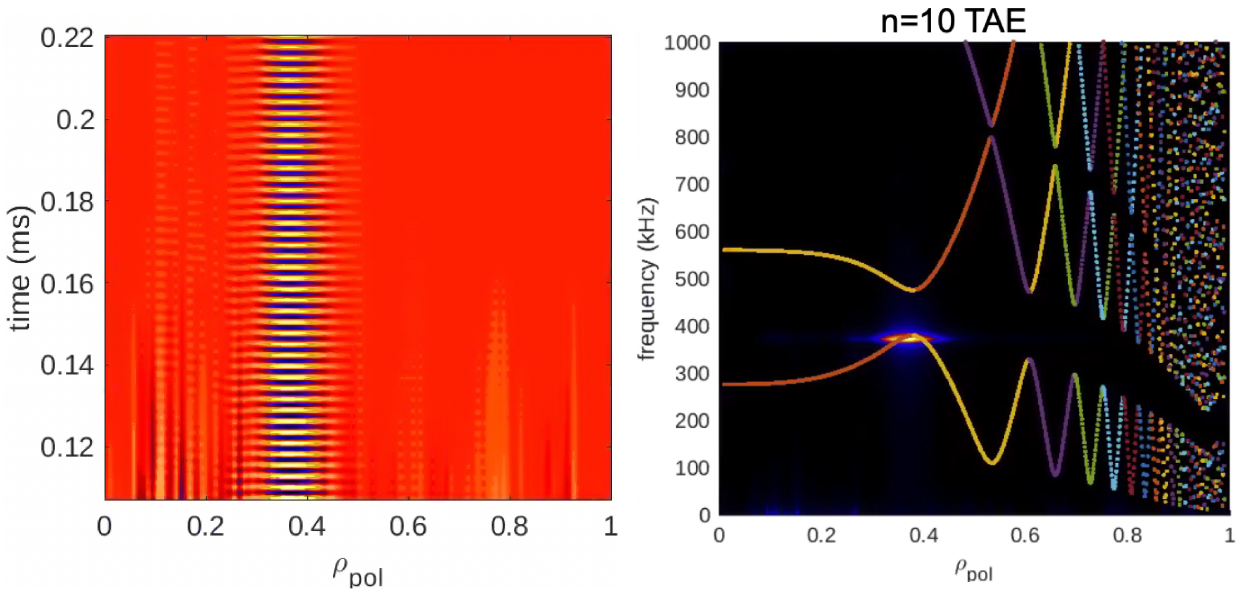

(a) (b)

Figure 6: MEGA: (a) Temporal evolution of the $n = 10$ radial velocity perturbation, δv_r, at the midplane during the linear phase. The mode amplitude is normalized by $\exp(-\gamma t_k)$ so that the mode location can be observed throughout the entire linear phase. (b) Fast Fourier Transform of the fields with the Shear Alfvén Wave continuum overplotted, showing the mode near the bottom of the TAE gap.

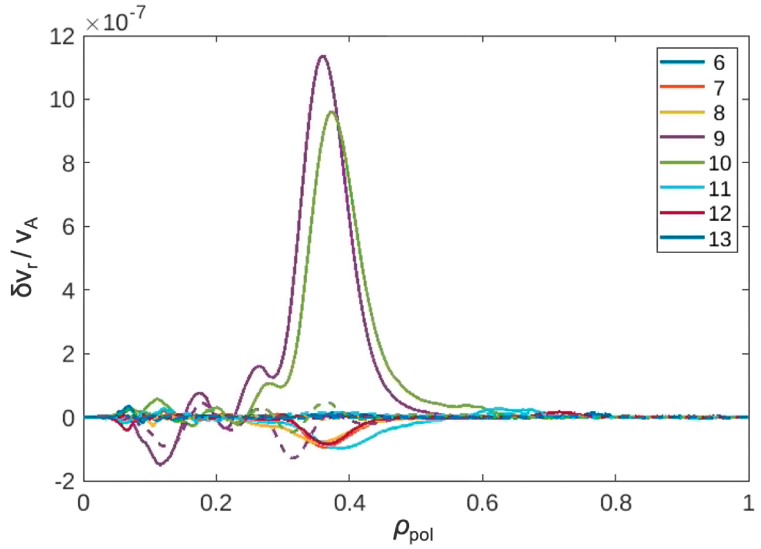

Figure 7: MEGA: Poloidal harmonics of the radial velocity δv_r for the $n = 10$ simulation, showing that $m = 9, 10$ dominate the simulation.

that its amplitude is comparable to the background numerical noise associated with these perturbative simulations. As the simulation progresses, the background noise level associated

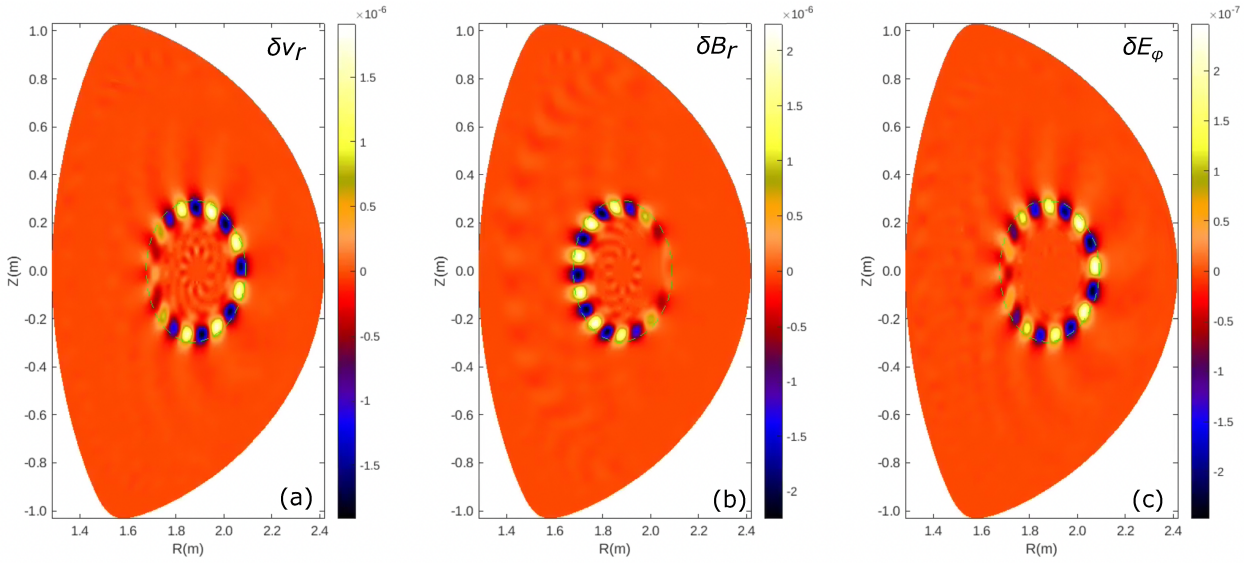

Figure 8: MEGA: The $n = 10$ TAE poloidal mode structure during the linear phase including all poloidal harmonics for the (a) radial velocity δv_r, (b) radial magnetic field δB_r, and (c) toroidal electric field δE_ϕ. For reference, the green dashed line corresponds to the location of the flux surface $\rho_{\text{pol}} = 0.4$.

with the $n = 0$ component becomes significant and, after $t = 0.22$ ms, induces the end of the simulation. When trying to mitigate this background noise inherent to the simulation by increasing the numerical resistivity from $\eta/(v_A R_0 \mu_0) = 5 \times 10^{-8}$ to 5×10^{-7}, the TAE is no longer visible, as its growth rate can also be affected by the value of the resistivity. Therefore, the TAE is characterized, but as it is marginally unstable, neither its saturated amplitude nor the associated relaxation of the alpha profile can be calculated self-consistently. The next section presents a scan in alpha pressure β_α that increases the growth rate so the instability can indeed saturate; however, because this is an artificially enhanced alpha profile, the associated relaxation of the alpha pressure profile is not discussed.

4.3. Alpha pressure scan

Because the described $n = 10$ simulations with the nominal alpha pressure profile, β_α from TRANSP/NUBEAM, do not produce a TAE unstable enough to saturate, the impact of uncertainties on the results needs to be investigated. Thus, a scan in alpha pressure and its gradient is executed to determine the sensitivity of stability with respect to changes in the alpha profile inputs.

For the pressure profile scans, we vary independently both the on-axis pressure $\beta_{\alpha 0}$ and the radial gradient of the profile. The radial gradient is modified ad-hoc by adjusting the exponent a of the poloidal flux, in Eq. (4), that determines the radial dependence of the weighting of the Monte Carlo markers. Figure 9a illustrates three different profiles (at constant $\beta_{\alpha 0}$) resulting by modifying this parameter. It is important to note that the pressure

remains constant at both the plasma axis as well as in the region near $\rho_{\rm pol} = 0.4$, where the TAE is destabilized. This means that, when scanning the gradient of alpha pressure, the actual pressure at the mode location remains approximately constant.

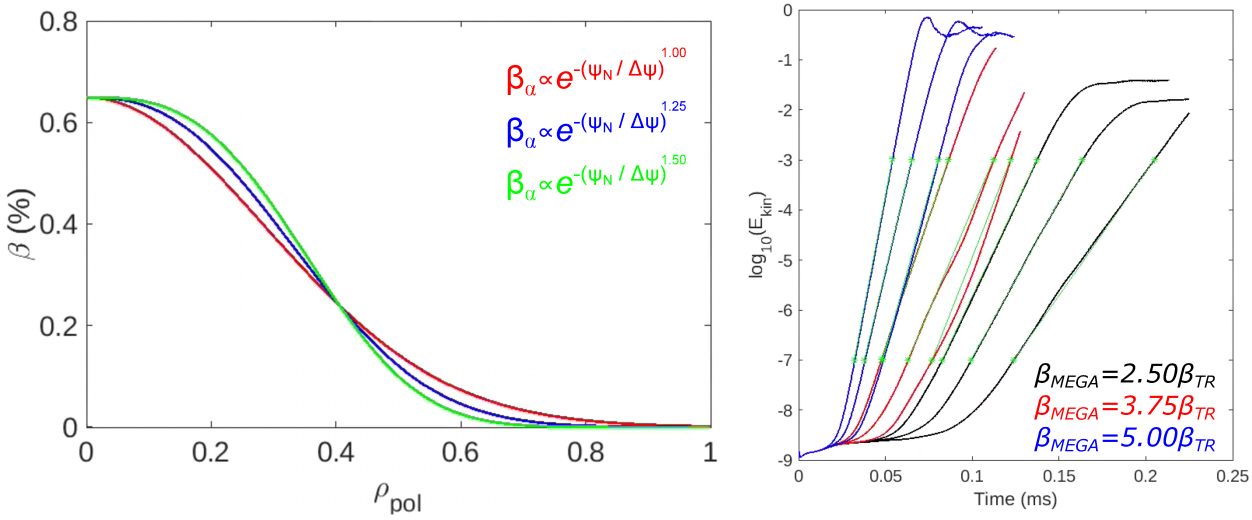

(a) (b)

Figure 9: MEGA:(a) Different radial profiles of the alpha particle pressure with different gradients used in the scan. (b) Evolution of the kinetic energy (log-scale) for simulations with different radial gradients and on-axis alpha pressures, scaled from the nominal alpha pressure from TRANSP $\beta_{\rm TR}$ (see Figs. 3a and 5a). The green points in (b) depict the time points used to calculate the growth rates of Table 2.

When increasing the pressure profile by a factor of two, the TAE still does not saturate, regardless of the gradient. It is observed that a factor of 2.5 needs to be applied to produce such saturation. Figure 9b depicts the temporal evolution of the kinetic energy of the $n = 10$ mode, on a logarithmic scale, when simulating alpha pressure profiles scaled by factors of 2.5, 3.75 and 5. For each scaling factor, three different curves correspond to the three radial gradients depicted in Fig. 9a. As expected, for each on-axis pressure, the steeper gradients produce faster instability growth.

The points where the kinetic energy reaches a normalized value of 10^{-7} and 10^{-3} are recorded to calculate the linear growth rates provided in Table 2. These time points are depicted as well in Fig. 9b, so it can be observed that the modes evolve nearly linearly, with some small deviations in the case $\beta_{\rm MEGA} = 3.75\beta_{\rm TR}$. For this case, a small interaction of the mode with the SAW continuum is observed. Other than that case, in these runs, no significant change in the TAE frequency nor location is observed, and the perturbation remains similar to Fig. 6b. Overall, it is found that the impact of the radial gradient on the growth rate is significant and can be comparable to scaling up the entire profile. In any case, to observe a TAE causing a strong alpha relaxation, the drive from the alpha population needs to be enhanced significantly.

Table 2: MEGA: Growth rates $\gamma/\omega > 0$ of the destabilized $n = 10$ TAE for different values of alpha pressure on axis $\beta_{\alpha 0}$, scaled from the TRANSP value β_{TR}, and radial gradient at the mode location, parameterized by $\beta_\alpha = \beta_{\alpha 0} \exp\left[-(\psi_N/\Delta\psi)^a\right]$. Here, ψ_{N} is the normalized poloidal flux, and $\Delta\psi = 0.16$ is the radial gradient scale length.

γ/ω (%)	$2.50\beta_{\mathrm{TR}}$	$3.75\beta_{\mathrm{TR}}$	$5.00\beta_{\mathrm{TR}}$
$a = 1.00$	1.06	1.90	2.70
$a = 1.25$	1.34	1.73	3.17
$a = 1.50$	1.57	2.21	3.94

Finally, we use the data in Table 2 to estimate the inherent mode damping in MEGA, as well as the nominal alpha drive. We consider the best-fit radial gradient ($a = 1$, see Fig. 5a) of the alpha pressure profile: $\beta_\alpha(\psi_{\mathrm{N}}) = \beta_{\alpha 0} \exp\left[-(\psi_{\mathrm{N}}/\Delta\psi)^a\right]$. By extrapolating the growth rate values to $\beta_{\alpha 0} = 0$, it is estimated that the intrinsic TAE damping in these simulations is $\gamma/\omega \approx -0.58\%$. Furthermore, extrapolating to the nominal TRANSP/NUBEAM value $\beta_{\alpha 0} = 0.65\%$, we find a total growth rate $\gamma/\omega \approx +0.08\%$, meaning the contribution of alpha drive is $\gamma/\omega \approx +0.66\%$ to this marginally unstable mode.

4.4. Toroidicity scan

The single-n simulations previously described focused on the $n = 10$ toroidicity because it is predicted to dominate by both Eq. (3) and the NOVA-K simulations reported in Section 3. To investigate the most unstable mode number, a scan in the toroidicity of the single-n simulation is performed. This scan already scales the alpha pressure profile by a factor, $5\beta_{TR}$, to save computational time and ensure that all simulated modes can overcome marginal stability and be characterized. The evolutions of the kinetic energies of this scan are shown in Fig. 10a. As a proxy for growth rate, the kinetic energy of the instabilities, for a single time point where all modes (except for $n = 5$) are growing linearly, is used and depicted in Fig. 10b.

From Figs. 10a and 10b, it is observed that the dominant instability is $n = 9$, followed by $n = 10$. As the simulated toroidicity deviates from these numbers, the TAE's growth rate and kinetic energy decrease, which is in general agreement with the NOVA-K results of Section 3 and Eq. (3). The $n = 9$ simulation was repeated using the same alpha pressure profile from TRANSP/NUBEAM, but similar results of marginal stability as $n = 10$ were found, as the mode was not able to self-consistently saturate.

5. Discussion

5.1. Similarities and agreement between NOVA-K and MEGA

While NOVA-K is a linear eigenvalue solver and MEGA is a nonlinear initial value code, it is encouraging that both find similar results for the SPARC PRD. First, the $n = 10$ Alfvén continua, computed by NOVA and ALCON, show similar features in Figs. 4 and 6b, with

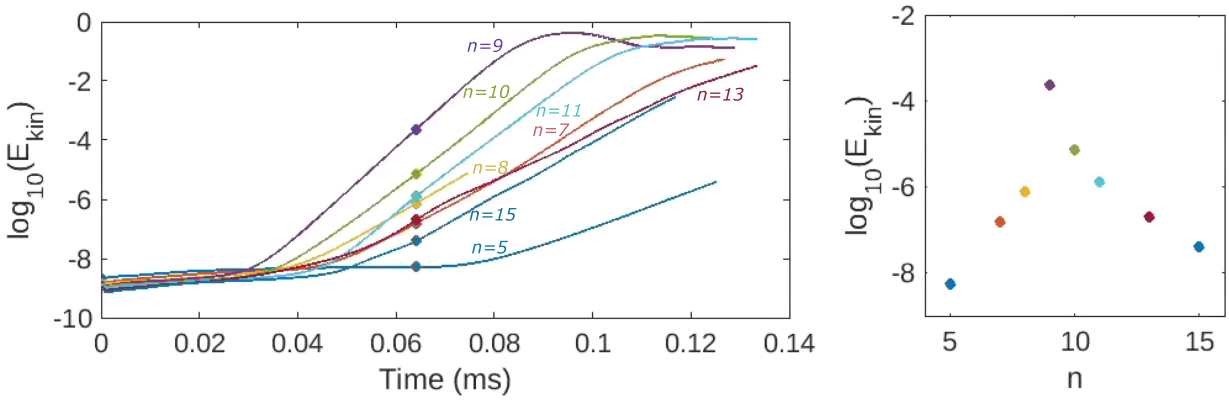

(a) (b)

Figure 10: MEGA: (a) Temporal evolution of the kinetic energy on a logarithmic scale for simulations with different toroidicities. (b) Kinetic energy, at $t = 0.65$ ms in (a), as a function of the toroidicity of each simulation.

a TAE gap which is open within $f \sim 300 - 500$ kHz throughout much of the plasma but becomes cut off near the edge. Small differences in the continua in the core and at the boundary may be due to slightly different treatments of the magnetic geometry there. As mentioned, the magnetic equilibrium is fit internally within NOVA-K, while MEGA uses a direct implementation; in a way, this replicates some "uncertainty" in the q profile, yet the results prove robust to these small changes.

The even-parity $n = 10$ TAE identified by NOVA-K and MEGA exhibit very similar poloidal mode structures, as seen in Figs. 4 and 7: the mode is localized near $\rho_{\rm pol} = \sqrt{\psi_{\rm N}} \sim 0.4$ with poloidal harmonics $m = 9, 10$ dominating. Again, there are small differences: The mode in MEGA is slightly shifted radially inward, $\rho_{\rm pol} < 0.4$, while that in NOVA-K is shifted slightly outward, $\rho_{\rm pol} > 0.4$. Moreover, the two eigenfrequencies differ by less than 10 kHz (<3%). These differences could again be due to small changes or uncertainties in the modeled q or density profiles.

Perhaps most important is the comparison of mode stability. For the even $n = 10$ TAE, NOVA-K predicts the mode to be stable (see Table 1), with mainly radiative damping ($\gamma/\omega = -1.35\%$) dominating over alpha drive when including FLR effects ($\gamma/\omega = +0.61\%$). MEGA, on the other hand, finds the mode to be marginally unstable ($\gamma/\omega = +0.08\%$), with a very similar contribution from alpha drive ($\gamma/\omega = +0.66\%$). It is perhaps unsurprising that the calculation of alpha drive is so similar between NOVA-K and MEGA since both codes treat the alpha population in almost identical ways. We also note here that the plasma profiles from TRANSP give a fusion power ~111 MW [19, 24], compared to the maximum expected 140 MW [9]; thus, it might be possible to have a ~25% increase in β_α and therefore also alpha drive for the PRD.

As discussed in Section 3, the RF-accelerated He3 minority population is calculated by NOVA-K to damp the TAEs; again this could be due to (i) the relatively low FI pressure

gradient at the mode location (see Fig. 3b) coupled with (ii) the a small fraction of He3 ions having velocities exceeding the Alfvén speed. The former is determined by RF power deposition, which has been evaluated to peak off axis ($\sqrt{\psi_N} \sim 0.2$) for more realistic RF antenna geometries [57] than the midplane position used here. Furthermore, other SPARC scenarios - such as L-mode plasmas with lower densities, higher RF powers (up to ∼25 MW), and perhaps lower He3 concentrations (<5%) - could lead to higher FI energies which could possibly drive TAEs. This scoping is left for further investigation.

Lastly, the toroidal mode number scan in MEGA ($n = 5-15$; see Fig. 10b) complements the coarse scan performed in NOVA-K ($n = 5, 10, 15, 20$; see Table 1): The most unstable mode number is evaluated to be $n^* = 9$ in MEGA and around $n^* \approx 10 - 15$ in NOVA-K. This also matches our expectation from theory (see Eq. (3)) where $n^* \approx 8 - 18$ for modes localized near $r/a \approx 0.5$. Due to limitations in computational resources, a larger range of n could not be scanned here; this is left to future work, which can further test the hypothesis of higher unstable mode numbers with increasing B_0 [11].

5.2. Differences and discrepancies between NOVA-K and MEGA

While the $n = 10$ TAE fluctuations are clear in Fig. 6a, the mode grows so slowly that the MEGA simulation does not reach the nonlinear phase unless the alpha pressure (β_α) profile and its gradient are significantly enhanced compared to the baseline values from TRANSP. By extrapolating the growth rate values of Table 2, the intrinsic damping rate of the instability is estimated to be $\gamma/\omega = -0.58\%$; this is ∼3× smaller than the damping rate predicted by NOVA-K for that instability, $\gamma/\omega = -1.48\%$, but ∼10× larger than the NOVA-K value for the higher frequency (odd) $n = 10$ mode, $\gamma/\omega = -0.05\%$ (see Table 1).

The damping in MEGA comes implicitly from the dissipative terms in the MHD equations: resistivity, viscosity, and diffusivity; NOVA-K, on the other hand, calculates each contribution from analytic theory. Landau and collisional damping would not be captured in MEGA, but they are predicted by NOVA-K to be small anyway. In this particular case, the $n = 10$ TAE has little-to-no intersection with the continuum, suggesting that the evaluation of mode coupling with the Alfvén continuum - i.e. radiative damping - is the primary discrepancy between the two codes. Some recent experiments [38, 58] have also identified the predominance of radiative damping on AEs in JET, and while NOVA-K simulations matched experimental measurements of net damping for a stable mode, MEGA was more successful at predicting the stability of all observed modes [38].

Thus, it is not clear which code best reflects reality. If NOVA-K is inaccurately assessing radiative damping, the even $n = 10$ TAE could outgrow the odd mode due the ∼2× larger alpha drive. Conversely, a different level of dissipation - e.g. via the resistivity - in MEGA might allow the high frequency mode to be most unstable. This illuminates one benefit of an eigenvalue code, which can identify the existence of all AE solutions, while an initial value code will only see the most destabilized modes. However, one particular challenge for NOVA-K is the computation time required to search through a wide range of eigenfrequencies

for these eigenmodes. Yet, once found, NOVA-K's explicit calculation of the many damping contributions allows us to probe individual physics mechanisms and attempt to propagate uncertainties analytically.

The MEGA simulations described in this manuscript have their limitations as well. For instance, the applied δf version of the code does not account for realistic particle generation or the He3 FI population generated by ICRH, which is left for future studies. Another limitation, which was previously mentioned, derives from the MHD description of the bulk plasma, as damping comes from the dissipation terms, not accounting for kinetic effects such as electron or thermal ion Landau damping. Yet MEGA's capabilities are also reflected in this work, as it has the flexibility to tune the alpha particle distribution function and self-consistently simulate, over time, the interaction between the alpha population and the waves destabilized in the bulk plasma.

6. Summary

In this work, we investigated the existence and stability of Toroidicity-induced Alfvén Eigenmodes (TAEs) in the DT "Primary Reference Discharge" (PRD) of the SPARC tokamak. The high magnetic field strength, $B_0 = 12.2$ T, is somewhat counteracted by the high plasma density, $n_{i0} > 10^{20}$ m^{-3} (see Fig. 1), to give an on-axis Alfvén speed $v_A \approx 9 \times 10^6$ m/s. SPARC's compact size ($R_0 = 1.85$ m, $a = 0.57$ m) and magnetic geometry (see Figs. 1a and 2) give rise to a TAE gap in the Alfvén continuum spanning $f \approx 300 - 500$ kHz (see Figs. 4 and 6b), at least for the expected "most unstable" toroidal mode numbers $n \approx 5 - 20$ (from Eq. (3)).

In the >100 MW, $Q \sim 9 - 11$ PRD, DT-fusion alphas provide most of the plasma self-heating (>20 MW) compared to RF-accelerated He3 minority species (∼11 MW). Yet, again due to strong B_0, the normalized pressure profiles are relatively low (see Fig. 3): the alpha pressure is $\beta_{\alpha 0} \approx 0.6\%$ on axis with a broad profile compared to the highly core-localized He3 minority. The alpha birth speed $v_{\alpha 0} \approx 1.3 \times 10^7$ m/s is larger than v_A, while only He3 ions with energies >1 MeV will exceed v_A. Thus, we expect that alphas will more readily destabilize TAEs in SPARC compared to He3 fast ions (FIs) due to the spatial profile/gradients and speed. However, variations in the safety factor (q) profile, e.g. due to the sawtooth instability, could change this.

Linear stability is first assessed with the eigenvalue solver NOVA-K. A coarse scan of $n = 5, 10, 15$ and 20 (only limited by computational resources) identifies even and odd eigenmodes at the bottom and top of the TAE gap, respectively, and localized primarily at the $q = 1$ surface (see Figs. 1a and 4). A stability analysis shows the high-frequency, odd $n = 10$ and 15 TAEs to be marginally destabilized, and the odd $n = 20$ only just marginally stabilized, while radiative damping dominates other modes (see Table 1). Interestingly but perhaps expectedly, the He3 FI population is predicted to *stabilize* the TAEs. Uncertainties in damping are assessed and can be significant, e.g. $\Delta\gamma/\omega \sim \pm 0.1\%$ for continuum and radiative damping. Similarly, the damping and drive from He3 FIs and alphas, respectively,

can be reduced by a factor up to ∼50% when including finite Larmor radius (FLR) effects. Nevertheless, the conclusions drawn on *net* TAE stability from NOVA-K remain effectively unchanged and are therefore robust to uncertainties.

The nonlinear evolution of TAEs is then modeled with initial value code MEGA. The alpha distribution function (see Fig. 5), fit with Eq. (4), marginally destabilizes an $n = 10$ TAE with frequency, location, and mode structure very similar to that in NOVA-K (see Figs. 6 to 8). Scans in the alpha pressure on axis and radial gradient at the mode location (see Fig. 9 and Table 2) simulate some uncertainty in the alpha profile; they also allow an extrapolation to assess the nominal alpha drive, $\gamma/\omega \approx +0.66\%$, which is very similar to that calculated by NOVA-K when including FLR effects (see Table 1), as well as the intrinsic damping, $\gamma/\omega \approx -0.58\%$, which is lower than the NOVA-K value. Lastly, a finer scan in toroidicity predicts $n = 9$ to be the true most unstable mode number (see Fig. 10).

The relatively good agreement between NOVA-K and MEGA simulations gives us confidence in the prediction of TAEs in the vicinity of $n \approx 10$ being most unstable for the SPARC PRD. Their marginal instability at the nominal alpha pressure is encouraging; that is, these TAEs are predicted to be only weakly driven and thus may not lead to significant alpha transport or confinement loss, thereby having little effect on overall plasma performance and fusion power. Furthermore, NOVA-K suggests that the (slightly) slower He3 minority species could further damp these TAEs, although this is still being assessed in ongoing MEGA simulations.

Ultimately, these results are an important starting point for future work: Of highest priority, perhaps, is a scan of other q profiles which, due to the sawtooth instability, will move the $q = 1$ surface - and TAE mode location - from the plasma axis to mid radius (the latter modeled here); as noted in Section 3, this will likely cause TAEs to disappear at the sawtooth crash, but then they may be strongly driven by larger FI betas and gradients near the core (see Fig. 3). In MEGA, we can also include RF-accelerated FIs (as mentioned) together with the alpha population, perform full-f multi-phase simulations [46,47], and assess nonlinear coupling of multiple AEs, perhaps even with the $n = 18$ ripple induced by the toroidal field coils. We also plan to explore AE-induced FI transport and loss, as well as the resulting impact on plasma performance via integrated modeling. The mode frequencies, structures, and locations identified in this work are also guiding diagnostic design for SPARC; for example, the high-frequency magnetic Mirnov coils.

Of course, the goal of this predictive simulation work is to validate models against future SPARC experiments for application to fusion power plants, like the ARC tokamak [59–62]. However, if TAEs are, in fact, only marginally destabilized for the SPARC PRD, we may need to rely on other plasma scenarios for AE stability investigation and validation: Lower B-field operations (8 T) will further lower the Alfvén speed v_A below the alpha birth velocity $v_{\alpha 0}$, likely increasing alpha drive; lower density operation, on the other hand, could raise $v_A > v_{\alpha 0}$, but may also lead to higher-energy minority populations, with $v_{\mathrm{FI}} > v_A$. Additionally, more realistic RF power deposition, slightly off-axis, may destabilize modes there. Finally, since alpha drive theoretically scales with q^2 [63–65], higher-q scenarios, albeit transient, could be

explored.

Acknowledgements

The authors thank N. Howard, M. Podestà, P. Rodridguez-Fernandez, and S. Scott for simulation support and fruitful discussions. We are also grateful to the reviewers whose feedback greatly improved this publication. J. Gonzalez-Martin is supported by the Juan de la Cierva Formación Fellowship FJC2021-047863-I and the project PID2020-116822RB-I00 funded by MICIU/AEI/10.13039/501100011033. R.A. Tinguely is supported by Commonwealth Fusion Systems. This research used resources of the National Energy Research Scientific Computing Center (NERSC), a Department of Energy Office of Science User Facility using NERSC awards FES-ERCAP-M3195 and FES-ERCAP-M3739.

References

[1] M. Garcia-Munoz, I.G.J. Classen, B. Geiger, W.W. Heidbrink, M.A. Van Zeeland, S. Äkäslompolo, R. Bilato, V. Bobkov, M. Brambilla, G.D. Conway, S. da Graça, V. Igochine, Ph. Lauber, N. Luhmann, M. Maraschek, F. Meo, H. Park, M. Schneller, G. Tardini, and the ASDEX Upgrade Team. Fast-ion transport induced by alfvén eigenmodes in the asdex upgrade tokamak. *Nuclear Fusion*, 51(10):103013, aug 2011.

[2] M. A. Van Zeeland, W. W. Heidbrink, R. K. Fisher, M. García Muñoz, G. J. Kramer, D. C. Pace, R. B. White, S. Aekaeslompolo, M. E. Austin, J. E. Boom, I. G. J. Classen, S. da Graça, B. Geiger, M. Gorelenkova, N. N. Gorelenkov, A. W. Hyatt, N. Luhmann, M. Maraschek, G. R. McKee, R. A. Moyer, C. M. Muscatello, R. Nazikian, H. Park, S. Sharapov, W. Suttrop, G. Tardini, B. J. Tobias, Y. B. Zhu, DIII-D, and ASDEX Upgrade Teams. Measurements and modeling of Alfvén eigenmode induced fast ion transport and loss in DIII-D and ASDEX Upgradea). *Physics of Plasmas*, 18(5):056114, 05 2011.

[3] C. S. Collins, W. W. Heidbrink, M. E. Austin, G. J. Kramer, D. C. Pace, C. C. Petty, L. Stagner, M. A. Van Zeeland, R. B. White, and Y. B. Zhu. Observation of critical-gradient behavior in alfvén-eigenmode-induced fast-ion transport. *Phys. Rev. Lett.*, 116:095001, Feb 2016.

[4] R Nazikian, G Y Fu, S H Batha, N N Gorelenkov, R V Budny, C E Bush, Z Chang, Y Chen, C Z Cheng, D S Darrow, P C Efthimion, E D Fredrickson, B Leblanc, R Majeski, E Mazzucato, F M Levinton, H K Park, M. Holthaus, J D Strachan, E J Synakowski, M V. Petrov, D A Spong, R B White, K L Wong, and S J Zweben. Alpha-Particle-Driven Toroidal Alfvén Eigenmodes in the Tokamak Fusion Test Reactor. *Physical Review Letters*, 78(15):2976–2979, 1997.

[5] R Nazikian, G J Kramer, C Z Cheng, N N Gorelenkov, H L Berk, and S E Sharapov. New interpretation of alpha-particle-driven instabilities in deuterium-tritium experiments on the tokamak fusion test reactor. *Physical Review Letters*, 91(12):125003–125004, 2003.

[6] M. Fitzgerald, R. Dumont, D. Keeling, J. Mailloux, S. Sharapov, M. Dreval, A. Figueiredo, R. Coelho, J. Ferreira, P. Rodrigues, F. Nabais, D. Borba, Ž. Štancar, G. Szepesi, R.A. Tinguely, P.G. Puglia, H.J.C. Oliver, V. Kiptily, M. Baruzzo, M. Lennholm, P. Siren, J. Garcia, C.F. Maggi, and JET Contributors. Stability analysis of alpha driven toroidal alfvén eigenmodes observed in jet deuterium-tritium internal transport barrier plasmas. *Nuclear Fusion*, 63(11):112006, oct 2023.

[7] P. Rodrigues, A. Figueiredo, J. Ferreira, R. Coelho, F. Nabais, D. Borba, N.F. Loureiro, H.J.C. Oliver, and S.E. Sharapov. Systematic linear-stability assessment of alfvén eigenmodes in the presence of fusion α-particles for iter-like equilibria. *Nuclear Fusion*, 55(8):083003, jun 2015.

[8] A.C.A. Figueiredo, P. Rodrigues, D. Borba, R. Coelho, L. Fazendeiro, J. Ferreira, N.F. Loureiro, F. Nabais, S.D. Pinches, A.R. Polevoi, and S.E. Sharapov. Comprehensive evaluation of the linear stability of alfvén eigenmodes driven by alpha particles in an iter baseline scenario. *Nuclear Fusion*, 56(7):076007, jun 2016.

[9] A. J. Creely, M. J. Greenwald, S. B. Ballinger, D. Brunner, J. Canik, J. Doody, T. Fülöp, D. T. Garnier, R. Granetz, T. K. Gray, C. Holland, N. T. Howard, J. W. Hughes, J. H. Irby, V. A. Izzo, G. J. Kramer, A. Q. Kuang, B. LaBombard, Y. Lin, B. Lipschultz, N. C. Logan, J. D. Lore, E. S. Marmar, K. Montes, R. T. Mumgaard, C. Paz-Soldan, C. Rea, M. L. Reinke, P. Rodriguez-Fernandez, K. Särkimäki, F. Sciortino, S. D. Scott, A. Snicker, P. B. Snyder, B. N. Sorbom, R. Sweeney, R. A. Tinguely, E. A. Tolman, M. Umansky, O. Vallhagen, J. Varje, D. G. Whyte, J. C. Wright, S. J. Wukitch, and J. Zhu. Overview of the SPARC tokamak. *Journal of Plasma Physics*, 86(5):865860502, oct 2020.

[10] Zachary S. Hartwig, , et al. The sparc toroidal field model coil program. *IEEE Transactions on Applied Superconductivity*, 34(2):1–16, 2024.

[11] E. A. Tolman, N. F. Loureiro, P. Rodrigues, J. W. Hughes, and E. S. Marmar. Dependence of alpha-particle-driven Alfvén eigenmode linear stability on device magnetic field strength and consequences for next-generation tokamaks. *Nuclear Fusion*, 59(4), mar 2019.

[12] G.T.A. Huysmans, J.P. Goedbloed, and W. Kerner. Isoparametric Bicubic Hermite Elements for Solution of the Grad-Shafranov Equation. *International Journal of Modern Physics C*, 02(01):371–376, 1991.

[13] A. B. Mikhailovskii, G. T. A. Huysmans, W. O. K. Kerner, and S. E. Sharapov. Optimization of computational MHD normal-mode analysis for tokamaks. *Plasma Physics Reports*, 23(10):844–857, 1997.

[14] Nabais F., Borba D., Coelho R., Figueiredo A., Ferreira J., Loureiro N., and Rodrigues P. The castor-k code, recent developments and applications. *Plasma Science and Technology*, 17(2):89, feb 2015.

[15] Elizabeth A. Tolman and Peter J. Catto. Drift kinetic theory of alpha transport by tokamak perturbations. *Journal of Plasma Physics*, 87(2):855870201, 2021.

[16] S. D. Scott, G. J. Kramer, E. A. Tolman, A. Snicker, J. Varje, K. Särkimäki, J. C. Wright, and P. Rodriguez-Fernandez. Fast-ion physics in sparc. *Journal of Plasma Physics*, 86(5):865860508, 2020.

[17] Jari Varje, Konsta Särkimäki, Joona Kontula, Patrik Ollus, Taina Kurki-Suonio, Antti Snicker, Eero Hirvijoki, and Simppa Äkäslompolo. High-performance orbit-following code ascot5 for monte carlo simulations in fusion plasmas, 2019.

[18] G J Kramer, R V Budny, A Bortolon, E D Fredrickson, G Y Fu, W W Heidbrink, R Nazikian, E Valeo, and M A Van Zeeland. A description of the full-particle-orbit-following spiral code for simulating fast-ion experiments in tokamaks. *Plasma Physics and Controlled Fusion*, 55(2):025013, jan 2013.

[19] P. Rodriguez-Fernandez, N. T. Howard, M. J. Greenwald, A. J. Creely, J. W. Hughes, J. C. Wright, C. Holland, Y. Lin, and F. Sciortino. Predictions of core plasma performance for the SPARC tokamak. *Journal of Plasma Physics*, 86(5):865860503, 2020.

[20] C.Z. Cheng. Kinetic extensions of magnetohydrodynamics for axisymmetric toroidal plasmas. *Physics Reports*, 211(1):1–51, 1992.

[21] G.Y. Fu and C.Z. Cheng. Excitation of high-n toroidicity-induced shear Alfvén eigenmodes by energetic particles and fusion alpha particles in tokamaks. *Physics of Fluids B: Plasma Physics*, 4(11):3722–3734, 1992.

[22] N.N. Gorelenkov, C.Z. Cheng, and G.Y. Fu. Fast particle finite orbit width and Larmor radius effects on low-n toroidicity induced Alfvén eigenmode excitation. *Physics of Plasmas*, 6(7):2802–2807, 1999.

[23] Y. Todo and T. Sato. Linear and nonlinear particle-magnetohydrodynamic simulations of the toroidal Alfvén eigenmode. *Physics of Plasmas*, 5:1321–1327, 1998.

[24] P. Rodriguez-Fernandez, A.J. Creely, M.J. Greenwald, D. Brunner, S.B. Ballinger, C.P. Chrobak, D.T. Garnier, R. Granetz, Z.S. Hartwig, N.T. Howard, J.W. Hughes, J.H. Irby, V.A. Izzo, A.Q. Kuang, Y. Lin, E.S. Marmar, R.T. Mumgaard, C. Rea, M.L. Reinke, V. Riccardo, J.E. Rice, S.D. Scott, B.N.

Sorbom, J.A. Stillerman, R. Sweeney, R.A. Tinguely, D.G. Whyte, J.C. Wright, and D.V. Yuryev. Overview of the sparc physics basis towards the exploration of burning-plasma regimes in high-field, compact tokamaks. *Nuclear Fusion*, 62(4):042003, mar 2022.

[25] J. Breslau, M. Gorelenkova, F. Poli, J. Sachdev, and X. Yuan. TRANSP. [Computer Software] https://doi.org/10.11578/dc.20180627.4, jun 2018.

[26] R.J. Hawryluk. An empirical approach to tokamak transport. In Coppi et al, editor, *Physics Close to Thermonuclear Conditions, Ed. B*, volume 19. Brussels: Commission of the European Communities, Brussels, 1980.

[27] J.P.H.E. Ongena, I. Voitsekhovitch, M. Evrard, and D. McCune. Numerical transport codes. *Fusion Science and Technology*, 61(2T):180–189, 2012.

[28] Y. Lin, J. C. Wright, and S. J. Wukitch. Physics basis for the icrf system of the sparc tokamak. *Journal of Plasma Physics*, 86(5):865860506, 2020.

[29] A. Pankin, D. McCune, R. Andre, G. Bateman, and A. Kritz. The tokamak Monte Carlo fast ion module NUBEAM in the National Transport Code Collaboration library. *Computer Physics Communications*, 159(3):157–184, 2004.

[30] M. Brambilla. Numerical simulation of ion cyclotron waves in tokamak plasmas. *Plasma Physics and Controlled Fusion*, 41(1):1–34, jan 1999.

[31] Gregory Wayne Hammett. *Fast ion studies of ion cyclotron heating in the PLT tokamak*. PhD thesis, Citeseer, 1986.

[32] J. A. Snipes, N. Basse, C. Boswell, E. Edlund, A. Fasoli, N. N. Gorelenkov, R. S. Granetz, L. Lin, Y. Lin, R. Parker, M. Porkolab, J. Sears, S. Sharapov, V. Tang, and S. Wukitch. Active and fast particle driven alfvén eigenmodes in alcator c-mod. *Physics of Plasmas*, 12(5):056102, 2005.

[33] W. W. Heidbrink. Alpha particle physics in a tokamak burning plasma experiment. In *Physics of Plasmas*, 2002.

[34] H. L. Berk, R. R. Mett, and D. M. Lindberg. Arbitrary mode number boundary-layer theory for nonideal toroidal Alfvén modes. *Physics of Fluids B*, 5(11):3969–3996, nov 1993.

[35] G. Y. Fu, C. Z. Cheng, R. Budny, Z. Chang, D. S. Darrow, E. Fredrickson, E. Mazzucato, R. Nazikian, K. L. Wong, and S. Zweben. Analysis of alpha particle-driven toroidal Alfvén eigenmodes in Tokamak Fusion Test Reactor deuterium-tritium experiments. *Physics of Plasmas*, 3(11):4036–4045, nov 1996.

[36] R. M. Nyqvist and S. E. Sharapov. Asymmetric radiative damping of low shear toroidal Alfvén eigenmodes. *Physics of Plasmas*, 19(8):082517, aug 2012.

[37] G. J. Kramer, S. E. Sharapov, R. Nazikian, N. N. Gorelenkov, and R. V. Budny. Observation of odd toroidal alfvén eigenmodes. *Physical Review Letters*, 92:4, 1 2004.

[38] R.A. Tinguely, J. Gonzalez-Martin, P.G. Puglia, N. Fil, S. Dowson, M. Porkolab, I. Kumar, M. Podestà, M. Baruzzo, A. Fasoli, Ye.O. Kazakov, M.F.F. Nave, M. Nocente, J. Ongena, Ž. Štancar, and JET Contributors. Simultaneous measurements of unstable and stable Alfvén eigenmodes in JET. *Nuclear Fusion*, 62(11):112008, 2022.

[39] R. R. Mett and S. M. Mahajan. Kinetic theory of toroidicity-induced Alfvén eigenmodes. *Physics of Fluids B*, 4(9):2885–2893, sep 1992.

[40] NN Gorelenkov and SE Sharapov. On the collisional damping of tae-modes on trapped electrons in tokamaks. *Physica Scripta*, 45(2):163, 1992.

[41] G.J. Kramer, C.Z. Cheng, Y. Kusama, R. Nazikian, S. Takeji, and K. Tobita. Magnetic safety factor profile before and after sawtooth crashes investigated with toroidicity and ellipticity induced alfvén eigenmodes. *Nuclear Fusion*, 41(9):1135, sep 2001.

[42] Jialei Wang, Yasushi Todo, Hao Wang, Zheng Xiong Wang, and Malik Idouakass. Stabilization of energetic-ion driven toroidal alfvén eigenmode by energetic electrons in tokamak plasmas. *Nuclear Fusion*, 60:106004, 8 2020.

[43] Hao Wang, Yasushi Todo, Masaki Oasakabe, Takeshi Ido, and Yasuhiro Suzuki. Simulation of energetic particle driven geodesic acoustic modes and the energy channeling in the large helical device plasmas. *Nuclear Fusion*, 59:096041, 8 2019.

[44] Y. Todo, M. A. Van Zeeland, A. Bierwage, and W. W. Heidbrink. Multi-phase simulation of fast ion profile flattening due to alfvén eigenmodes in a diii-d experiment. *Nuclear Fusion*, 54, 2014.

[45] Y. Todo, M. A. Van Zeeland, A. Bierwage, W. W. Heidbrink, and M. E. Austin. Validation of comprehensive magnetohydrodynamic hybrid simulations for alfvén eigenmode induced energetic particle transport in diii-d plasmas. *Nuclear Fusion*, 55, 2015.

[46] Y. Todo, M. A. Van Zeeland, and W. W. Heidbrink. Fast ion profile stiffness due to the resonance overlap of multiple alfvén eigenmodes. *Nuclear Fusion*, 56, 2016.

[47] Andreas Bierwage, Kouji Shinohara, Yasushi Todo, Nobuyuki Aiba, Masao Ishikawa, Go Matsunaga, Manabu Takechi, and Masatoshi Yagi. Simulations tackle abrupt massive migrations of energetic beam ions in a tokamak plasma. *Nature Communications*, 9:1–11, 12 2018.

[48] X.D. Du, M.A. Van Zeeland, W.W. Heidbrink, J. Gonzalez-Martin, K. Särkimäki, A. Snicker, D. Lin, C.S. Collins, M.E. Austin, G.R. McKee, Z. Yan, Y. Todo, and W. Wu. Visualization of fast ion phase-space flow driven by alfvén instabilities. *Physical Review Letters*, 127:235002, 12 2021.

[49] J. Gonzalez-Martin, X. D. Du, W. W. Heidbrink, M. A. Van Zeeland, K. Särkimäki, A. Snicker, X. Wang, and Y. Todo. Modelling the alfvén eigenmode induced fast-ion flow measured by an imaging neutral particle analyzer. *Nuclear Fusion*, 62:112003, 9 2022.

[50] X. Du, W. Heidbrink, M. Van Zeeland, J. Gonzalez-Martin, M. Austin, Z. Yan, and G. McKee. Visualization of fast ion phase-space flow in plasmas well-below, near and well-above alfvén eigenmode stability threshold in tokamak. *Nuclear Fusion*, 63:046020, 3 2023.

[51] M. A. Van Zeeland, L. Bardoczi, J. Gonzalez-Martin, W. W. Heidbrink, M. Podesta, M. Austin, C. S. Collins, X. D. Du, V. N. Duarte, M. Garcia-Munoz, S. Munaretto, K. E. Thome, Y. Todo, and X. Wang. Beam modulation and bump-on-tail effects on alfvén eigenmode stability in diii-d. *Nuclear Fusion*, 61:066028, 5 2021.

[52] Active control of alfvén eigenmodes by externally applied 3d magnetic perturbations. *Physical Review Letters*, 130:035101, 1 2023.

[53] J. Gonzalez-Martin, M. Garcia-Munoz, J. Galdon-Quiroga, Y. Todo, J. Dominguez-Palacios, M. Dunne, A. Jansen Van Vuuren, Y. Q. Liu, L. Sanchis-Sanchez, D. Spong, W. Suttrop, X. Wang, and M. Willensdorfer. Active control of alfvén eigenmodes by external magnetic perturbations with different spatial spectra. *Nuclear Fusion*, 64:076022, 6 2024.

[54] Hao Wang and Yasushi Todo. Linear properties of energetic particle driven geodesic acoustic mode. *Physics of Plasmas*, 20, 1 2013.

[55] W. Deng, Z. Lin, I. Holod, Z. Wang, Y. Xiao, and H. Zhang. Linear properties of reversed shear Alfvén eigenmodes in the DIII-D tokamak. *Nuclear Fusion*, 52(4):043006, 2012.

[56] S. D. Pinches, I. T. Chapman, Ph W. Lauber, H. J.C. Oliver, S. E. Sharapov, K. Shinohara, and K. Tani. Energetic ions in iter plasmas. *Physics of Plasmas*, 22, 2 2015.

[57] Gregory Wallace, Christina Migliore, John Wright, Michael Brookman, and Michael Garrett. Retiring risk for ion cyclotron range of frequency heating in sparc through modeling. In *APS Division of Plasma Physics Meeting Abstracts*, volume 2023, pages NO05–008, 2023.

[58] R.A. Tinguely, P.G. Puglia, S. Dowson, M. Porkolab, D. Douai, A. Fasoli, L. Frassinetti, D. King, P. Schneider, and JET Contributors. Isotope effects and alfvén eigenmode stability in jet h, d, t, dt, and he plasmas. *Nuclear Fusion*, 64(9):096002, jul 2024.

[59] B.N. Sorbom, J. Ball, T.R. Palmer, F.J. Mangiarotti, J.M. Sierchio, P. Bonoli, C. Kasten, D.A. Sutherland, H.S. Barnard, C.B. Haakonsen, J. Goh, C. Sung, and D.G. Whyte. Arc: A compact, high-field, fusion nuclear science facility and demonstration power plant with demountable magnets. *Fusion Engineering and Design*, 100:378–405, 2015.

[60] A.Q. Kuang, N.M. Cao, A.J. Creely, C.A. Dennett, J. Hecla, B. LaBombard, R.A. Tinguely, E.A. Tolman, H. Hoffman, M. Major, J. Ruiz Ruiz, D. Brunner, P. Grover, C. Laughman, B.N. Sorbom, and D.G. Whyte. Conceptual design study for heat exhaust management in the arc fusion pilot plant. *Fusion Engineering and Design*, 137:221–242, 2018.

[61] Alexander Creely, Devon Battaglia, Michael Brookman, Dan Brunner, Chris Chrobak, Nathan Howard,

Adam Kuang, Tom Looby, Robert Mumgaard, Anders Oberg, et al. Demonstration of fusion pilot plant physics in sparc. In *APS Division of Plasma Physics Meeting Abstracts*, volume 2022, pages NO03–003, 2022.

[62] Jon Hillesheim, Alex Creely, Devon Battaglia, Tom Body, M Brookman, Dan Brunner, Thomas Eich, Nathan Howard, Adam Kuang, Tom Looby, et al. Arc physics basis status. In *APS Division of Plasma Physics Meeting Abstracts*, volume 2023, pages JP11–115, 2023.

[63] G Y Fu and J W Van Dam. Excitation of the toroidicity-induced shear Alfvén eigenmode by fusion alpha particles in an ignited tokamak. *Physics of Fluids B: Plasma Physics*, 1:1949, 1989.

[64] C. Z. Cheng. Alpha particle destabilization of the toroidicity-induced Alfvén eigenmodes. *Physics of Fluids B: Plasma Physics*, 3(9):2463–2471, 09 1991.

[65] B N Breizman and S E Sharapov. Energetic particle drive for toroidicity-induced Alfven eigenmodes and kinetic toroidicity-induced Alfven eigenmodes in a low-shear tokamak. *Plasma Physics and Controlled Fusion*, 37(10):1057, oct 1995.